

This discussion paper is/has been under review for the journal Atmospheric Chemistry and Physics (ACP). Please refer to the corresponding final paper in ACP if available.

Limited-area modelling of stratocumulus over South-Eastern Pacific

M. Andrejczuk¹, W. W. Grabowski², A. Gadian¹, and R. Burton¹

¹School of Earth and Environment, University of Leeds, Leeds LS2 9JT, UK

²National Center for Atmospheric Research, Boulder, Colorado, USA

Received: 23 August 2011 – Accepted: 2 September 2011 – Published: 12 September 2011

Correspondence to: M. Andrejczuk (m.andrejczuk@leeds.ac.uk)

Published by Copernicus Publications on behalf of the European Geosciences Union.

ACPD

11, 25517–25556, 2011

Limited-area modelling of stratocumulus over South-Eastern Pacific

M. Andrejczuk et al.

Title Page

Abstract

Introduction

Conclusions

References

Tables

Figures

⏪

⏩

◀

▶

Back

Close

Full Screen / Esc

Printer-friendly Version

Interactive Discussion



Abstract

This paper discusses the application of the Weather Research and Forecasting (WRF) model to limited-area modeling of atmospheric processes over the subtropical south-eastern Pacific, with the emphasis on the stratocumulus-topped boundary layer. The simulations cover a period of 42 h selected from the VAMOS (Variability of the American Monsoon Systems) Ocean-Cloud-Atmosphere-Land Study Regional Experiment (VOCALS-REx) field project conducted in the subtropical south-eastern Pacific in October and November 2008. Modeling results are compared with aircraft observations with the main conclusion that the simulated stratocumulus-topped boundary layer is significantly too shallow. This appears to be a combination of an already too shallow boundary layer in the dataset used to provide initial and lateral boundary conditions, and deficiencies of the boundary-layer scheme in the WRF model. We suggest that the latter comes from the scheme confusing the cloud base change of the vertical temperature and moisture gradients with the change at the boundary-layer inversion. The model does simulate the formation of mesoscale cloud-free regions, arguably similar to Pockets of Open Cells observed in nature. In the model, formation of these regions does not seem to be related to drizzle-induced transition from open- to closed-cell circulations as simulated by LES models. Instead, the cloud-free regions appear to result from mesoscale variations of the lower-tropospheric vertical velocity. Areas of negative vertical velocity with minima near the boundary layer top (a few cm s^{-1}) seem to induce direct evaporation of the cloud layer. Parameterized boundary entrainment may play some role as well. It remains to be seen in LES studies whether the mechanism seen in the limited-area model is realistic or if it is simply an artifact of interactions between resolved and parameterized processes.

Limited-area modelling of stratocumulus over South-Eastern Pacific

M. Andrejczuk et al.

Title Page

Abstract

Introduction

Conclusions

References

Tables

Figures



Back

Close

Full Screen / Esc

Printer-friendly Version

Interactive Discussion



1 Introduction

Numerical models are the only tools that can be used to objectively predict evolution of the state of the atmosphere. However, due to limited spatial and temporal resolutions, these models require parametrizations of unresolved processes. As a result, the model solutions depend not only on the initial and boundary conditions as well as on spatial and temporal resolutions, but also on specific parametrizations applied in the simulations. This especially applies to limited-area modeling because of the disparity between model horizontal gridlength (typically ~ 10 km) and gridlengths required to resolve boundary-layer processes, turbulent transports in particular. The VAMOS (Varaibility of the American Monsoon Systems) Ocean-Cloud-Atmosphere-Land Study Regional Experiment (VOCALS-REx) field project conducted in the subtropical south-eastern Pacific in October and November 2008 (Wood et al., 2011b) provided copious data for model evaluation and validation. The atmospheric conditions in this region are determined by the large-scale free-tropospheric subsidence and low sea surface temperature (SST). Similarly to the subtropical region off the California coast, such conditions lead to a cold well-mixed boundary layer topped by a persistent stratocumulus deck (Rahn and Garreaud, 2010; Toniazzo et al., 2011). Due to a large area of coverage and persistence of stratocumulus clouds, this region significantly affects planetary albedo. It follows that accurate predictions of macroscopic (e.g. cloud fraction) as well as microscopic (e.g. cloud droplet size) properties of these clouds are important not only from the weather prediction point of view, but also from the climate perspective. Such concerns provided the primary motivation for the VOCALS-REx field experiment.

Stratocumulus decks off the California coast and over the southeastern Pacific often show dramatic changes in the boundary layer cloudiness, from almost solid cloud cover associated with the so-called closed cells to partially-cloudy regions of open cells embedded within the closed-cell expanse. The open-cell structures are called Pockets of Open Cells (POCs) (Stevens et al., 2005) or rifts (Sharon et al., 2006). Their origin is not fully understood, but significant differences in aerosol and cloud microphysical

Limited-area modelling of stratocumulus over South-Eastern Pacific

M. Andrejczuk et al.

Title Page

Abstract

Introduction

Conclusions

References

Tables

Figures



Back

Close

Full Screen / Esc

Printer-friendly Version

Interactive Discussion



**Limited-area
modelling of
stratocumulus over
South-Eastern Pacific**

M. Andrejczuk et al.

[Title Page](#)[Abstract](#)[Introduction](#)[Conclusions](#)[References](#)[Tables](#)[Figures](#)[Back](#)[Close](#)[Full Screen / Esc](#)[Printer-friendly Version](#)[Interactive Discussion](#)

properties between POCs and the surrounding clouds are typically observed (VanZanten and Stevens, 2005; Petters et al., 2006; Sharon et al., 2006; Wood et al., 2008, 2011a). VanZanten and Stevens (2005), Sharon et al. (2006), and Wood et al. (2011a) found that POCs are characterized by enhanced drizzle, although drizzle itself seem insufficient for transition from closed- to open-cell circulations Wood et al. (2011a).

Specific reasons for transitions from closed- to open-cell structure are difficult to determine from observations, and as a result large-eddy simulation (LES) numerical models are often used to investigate the transition (e.g. Savic-Jovicic and Stevens, 2008; Wang and Feingold, 2009a,b; Wang et al., 2010). Model simulations indicate that drizzle can trigger POC formations and subsequently accelerate this process by aerosol depletion, thus pointing to the importance of cloud-aerosol interactions. A recent study by Abel et al. (2010) shows that a model with a relatively low spatial resolution (horizontal gridlength of 17 km) is able to create cloud-free region within the solid stratocumulus deck. Although it is unclear whether the mechanisms in the numerical model are the same as in nature, the presence of cloud-free regions in the low-resolution model indicates that processes other than cloud-aerosol interactions (such as mesoscale waves, for instance) may also be important for transition from closed- to open-cell circulations.

LES models are typically run with gridlengths of a few tens of meters in order to resolve boundary-layer eddies and the stratocumulus cloud that is often only a couple of hundred meters thick. Often even higher vertical resolution is used to better represent the sharp temperature and moisture inversion near the top of the boundary layer and entrainment/mixing processes across the inversion. However, the high spatial resolution implies that only a relatively small area (up to a few hundred km²) can be modeled using LES approach. Moreover, the effects of variable (in space and time) large-scale conditions are difficult to impose, and the interactions between small-scale (boundary-layer) processes and the larger-scale dynamics (e.g. mesoscale free-tropospheric waves) cannot be considered. Arguably, such interactions can impose significant forcing on the boundary layer, and on the stratocumulus cloud in particular.

Limited-area modelling of stratocumulus over South-Eastern Pacific

M. Andrejczuk et al.

Title Page

Abstract

Introduction

Conclusions

References

Tables

Figures

⏪

⏩

◀

▶

Back

Close

Full Screen / Esc

Printer-friendly Version

Interactive Discussion



This paper presents an application of the Weather Research and Forecasting (WRF) model (Skamarock et al., 2008) to the 13 November VOCALS-REx case. The WRF model was run in the limited-area mode with the horizontal gridlength of several kilometers and covering a significant fraction of the subtropical southeastern Pacific (SEP).

Model results (the lower tropospheric structure in particular) are compared to the observations taken by the BAe-146 UK research aircraft. Sensitivity of model solutions to the number of vertical levels, boundary layer and microphysics parameterizations, and to the horizontal resolution is also explored. The model does simulate the formation of cloud-free regions in the stratocumulus deck and details of the transition from a cloudy to cloud-free boundary layer are investigated.

The next section discusses the numerical model setup, as well as initial and boundary conditions. The WRF model solutions with different parameterizations are compared to the aircraft observations in Sect. 3. Section 4 discusses simulated mechanisms behind the formation of cloud-free regions. A brief discussion and conclusions are presented in Sect. 5.

2 Numerical model

The WRF model (Skamarock et al., 2008) was used to simulate evolution of the stratocumulus clouds over SEP region applying two nested domains. Global Forecast System (GFS) analyses (1 degree horizontal resolution) were used to prescribe initial and boundary conditions for WRF simulations. Spatial and temporal SSTs variations were obtained (i.e. interpolated in space and time) from 6-hourly GFS values. The WRF model was initialized at 00:00 UTC on 12 November and run for 42 h. Model output was saved every 15 min starting from 06:00 on 13 November. The outer model domain applied a 9-km grid with 312×212 gridpoints in the E-W and N-S direction, with the centre of the computational domain was located at 20° S and 80° W. The inner domain used a 3-km grid with 380×142 gridpoints. It was placed in such a way that its SW corner was located at a gridpoint (80, 90) of the outer domain. The inner domain

was initialized from the outer domain solution at 00:00 UTC of 13 November, that is, after 24 h of the outer-domain simulation.

The default WRF vertical setup features 36 vertical levels, with the first model level at 29 m and the vertical gridlength around 343 m at the height of 1.4 km (where the cloud top was observed). Such a vertical gridlength is likely to be too large to simulate a realistically cloud-topped boundary layer. To investigate how the model responds to the change of the vertical resolution and the number of vertical levels, two additional simulations were performed, one using 81 levels (eta levels from 0 to 1 by 0.0125) and the second one using 121 levels (eta levels from 0 to 1 by 0.00833). Applying 81/121 levels results in the height of the first level above the surface of 51/34 m, and the vertical gridlength of 120/81 m near the observed cloud top.

Because of the relatively coarse model resolution, especially from the point of view of boundary-layer processes, subgrid-scale parameterizations play an important role in the simulations. The suite of subgrid-scale parameterizations involve the formulation of surface fluxes, convective transports within the boundary layer as well as cloud microphysics associated with the stratocumulus cloud. In addition, a land-surface model is applied because the computational domain includes a small fraction of the South American continent (see Fig. 1). The following parametrizations were used in the simulations:

– PBL models:

a. The ACM2 (Asymmetric Convective Model, version 2) scheme uses local closure in stable and combined local and non-local closures in unstable conditions.

b. The YSU (Yonsei University) scheme uses a counter-gradient approach to represent transports due to unresolved boundary-layer eddies and an explicit treatment of entrainment processes at the top of the PBL.

c. The MYJ (Mellor-Yamada-Janjiic) scheme calculates eddy diffusion coefficients from the prognostic TKE equation. This scheme uses Mellor-Yamada Level 2.5 turbulence (local) closure model.

**Limited-area
modelling of
stratocumulus over
South-Eastern Pacific**

M. Andrejczuk et al.

Title Page

Abstract

Introduction

Conclusions

References

Tables

Figures



Back

Close

Full Screen / Esc

Printer-friendly Version

Interactive Discussion



Limited-area modelling of stratocumulus over South-Eastern Pacific

M. Andrejczuk et al.

Title Page

Abstract

Introduction

Conclusions

References

Tables

Figures



Back

Close

Full Screen / Esc

Printer-friendly Version

Interactive Discussion



– Land surface models:

a. NOAA Land Surface Model is a 4 layer soil temperature and soil moisture model with predictive canopy moisture and snow cover.

b. Thermal diffusion scheme predicts temperature for 5 soil levels. Soil moisture is specified based on the land use and season.

– Surface layer models:

a. Monin-Obukhov (MO) scheme uses MO similarity theory to derive profiles of the wind and temperature in the surface layer.

b. ETA-model implementation of the MO scheme adds representation of the viscous sub-layer.

c. Pleim-Xiu scheme is based on similarity theory. A quasi-laminar sublayer is introduced to account for the difference between momentum and scalar fluxes. The MO stability parameter z/L for stable and unstable conditions is derived from the bulk Richardson number. A correction function for very stable conditions is modified to avoid decoupling from the surface. The correction is a function of z/L (the bulk Richardson number) for stable (unstable) conditions.

– Microphysics models:

a. The Kessler war-rain bulk microphysics.

b. The Thompson microphysics predicts mixing ratios of the cloud water, rain, cloud ice, snow, and graupel; and cloud ice number concentration. The scheme uses generalized gamma distribution for each hydrometeor species. The cloud droplet number concentration is assumed 300 cm^{-3} .

c. The Morrison 2-moment bulk microphysics scheme predicts the number concentrations and the mixing ratios of the cloud ice, rain, snow, groupel (or hail) and mixing ratio of cloud droplets; a gamma distribution is used to describe shape of the hydrometeors distribution. Cloud droplet number concentration is assumed 300 cm^{-3} .

– Radiation transfer models:

a. Longwave radiation: The RRTM (Rapid Radiative Transfer Model) is a spectral band scheme using the correlated k method. This scheme calculates fluxes and cooling rates for the longwave spectral region (10–3000 cm^{-1}). It takes into account water vapor, cloud water, carbon dioxide, ozone, methane, nitrous oxide, and common halocarbons.

b. Shortwave radiation: the Goddard scheme divides the solar spectrum into 8 bands in the UV and visible range. The scheme accounts for the scattering by the atmospheric gases, clouds and aerosols, and for the absorption by the ozone, water vapor, oxygen and carbon dioxide.

Table 1 provides more details concerning parametrizations used in the simulations. Specific references are provided in Skamarock et al. (2008).

3 VOCALS-REx aircraft observations

Observations used for model evaluation were taken by the BAe-146 research aircraft on 13 November 2008 (flight B420). Figure 1 shows the B420 flight track. Profiles at 6 locations, shown in the figure, were selected for model evaluation. Each of these profiles is obtained through a relatively rapid sampling of the lower troposphere, with 5 descents from above the cloud to near the ocean surface (in locations 1 to 5) and one ascent (location 6) from near the surface to the altitude of about 7.5 km. Each of these profiles is assigned to a spatial location in the closest-in-time model output. Other aircraft profiles on that day are either too close to the coast (such profiles are likely affected by poorly resolved land-sea circulations) or do not reach the cloud top.

The 1-Hz data collected during the flight are used to obtain profiles of various variables. The potential temperature is derived using the temperature from the Rosemount deiced sensor and the pressure from the aircraft Reduced Vertical Separation Minimum (RVSM) system. The water vapor mixing ratio is derived from the dew point temperature obtained from the TWC (Total Water Content) probe. The cloud water mixing ratio

Limited-area modelling of stratocumulus over South-Eastern Pacific

M. Andrejczuk et al.

Title Page

Abstract

Introduction

Conclusions

References

Tables

Figures



Back

Close

Full Screen / Esc

Printer-friendly Version

Interactive Discussion



is estimated from the Nevzorov probe, and the air velocity components are obtained from the turbulence probe and GIN (GPS-aided Inertial Navigation) unit. Profiles of these variables are compared to model profiles using the approximate time-and-space location of the model output. Additional data (i.e. from gray segments in the right panel of Fig. 1) are used to show the variability of the atmospheric structure in the vicinity of main profile locations. The difference between the main profile and additional profiles (or partial profiles) is a measure of the representativeness of the profiles and provides a reference for the difference between the model results and the observations.

4 Results

4.1 Model evaluation and sensitivity

Figures 2 to 7 show profiles derived from observed variables (temperature, moisture and wind) for locations 1 to 6, respectively, and model results for time/space locations approximately corresponding to the profiles. For profiles 1 to 3, the figures show model results with different vertical grids (i.e. increasing the number of model levels), whereas results from simulations applying 81 levels and different parameterizations of boundary-layer processes are shown in Figs. 5 to 7. Additional observational data (e.g. partial profiles) as described above are also shown in the figures.

Figures 2 to 7 clearly show that the model severely underestimates the depth of the boundary layer. The observed top of the approximately well-mixed boundary layer is between 1 and 1.5 km, but the model predicts the depth of between 0.5 and 1 km. Additional data points (gray symbols) show some variability of temperature and moisture profiles, but not the boundary layer depth. Note that the model does produce stratocumulus cloud despite the much shallower boundary layer. This implies that that the modeled boundary layer has to be either colder or more humid than observed, or both. Inspection of the figures suggests that, typically, the boundary layer is too moist (see Figs. 3, 4, and 5), although in some locations it is also slightly colder (e.g.

**Limited-area
modelling of
stratocumulus over
South-Eastern Pacific**

M. Andrejczuk et al.

Title Page

Abstract

Introduction

Conclusions

References

Tables

Figures



Back

Close

Full Screen / Esc

Printer-friendly Version

Interactive Discussion



**Limited-area
modelling of
stratocumulus over
South-Eastern Pacific**

M. Andrejczuk et al.

Title Page

Abstract

Introduction

Conclusions

References

Tables

Figures

⏪

⏩

◀

▶

Back

Close

Full Screen / Esc

Printer-friendly Version

Interactive Discussion

Figs. 2 and 5). Considering the poor simulation of the boundary layer depth, it is not surprising that the maximum values of the cloud water mixing ratio q_c are different in the observations and the model solutions. There is, however, no consistent trend, and the model maximum of the cloud water mixing ratio is in some locations higher than observed and sometimes it is lower, with some model profiles showing no cloud water. There are also significant differences between observed and modeled horizontal velocity components. In particular, the observed wind profiles show significantly higher short-vertical-wavelength variability below the mixed-layer inversion. Arguably, such fluctuations come from instantaneous probing of small-scale atmospheric circulations within the boundary layer that the model is not able to simulate because of low spatial resolution. The differences between various observed velocity profiles in the proximity of the same location (i.e. the difference between black and gray symbols) is relatively large. This implies a sizeable time and space variability of the horizontal velocity and suggests that velocity differences between model and observations are less significant than in the cases of the temperature and moisture profiles.

Figures 2 to 4 also show profiles from simulations applying an increased number of vertical levels, 81 and 121. Increasing the number of levels does improve the temperature and moisture profiles as the boundary layer depth increases when the number of model levels is increased, but the depth is still too small even with the largest number of levels when compared to the observations. The same conclusion applies to the comparison between simulated and observed profiles at locations 4 to 6 (not shown). The impact of the increased number of levels on the lower-tropospheric winds is rather small, except for the profile 1 shown in Fig. 2, where the increase in the number of levels leads to a significant change of the zonal wind component. This is perhaps because profile 1 is the closest to the land and imperfections in the representation of circulations in the vicinity of the coastline are responsible.

The WRF model offers several parameterizations of the land-surface and boundary-layer processes. The control simulation REF applied Pleim-Xiu surface layer and ACM2 boundary layers parameterizations. The sensitivity simulations SF1 used

**Limited-area
modelling of
stratocumulus over
South-Eastern Pacific**

M. Andrejczuk et al.

[Title Page](#)[Abstract](#)[Introduction](#)[Conclusions](#)[References](#)[Tables](#)[Figures](#)[Back](#)[Close](#)[Full Screen / Esc](#)[Printer-friendly Version](#)[Interactive Discussion](#)

Monin-Obukhov surface layer and YSU boundary layer parameterizations; and SF2 used ETA version of the Monin-Obukhov surface layer and MYJ TKE boundary-layer parameterizations. Arguably, one might expect that application of a different surface and boundary-layer parameterizations could lead to an improved solutions. Figures 5 to 7, in the same format as Figs. 2 to 4, show solutions corresponding to the observational profiles 4 to 6, respectively, from the simulations applying 81 vertical levels and three setups differing in the way surface fluxes are calculated and distributed within the boundary layer. As in previous figures, black lines show the observed profiles and gray points document the variability of the observations within 30 min of the profile measurements being taken. The results show that the combination of parameterizations used in the reference run REF gives profiles of potential temperature and water vapour mixing ratio closest to the observations. The two other sensitivity simulations tend to predict even shallower well-mixed boundary layer. The impact on the horizontal velocity profiles is comparable to the impact of the vertical resolution. Profiles of θ and q_v , unlike the horizontal wind, agree relatively well above the boundary layer.

Two sensitivity simulations applying 81 vertical levels were also run with the simple Kessler cloud microphysics replaced with either the Thompson et al. (2004) or Morrison et al. (2009) microphysics scheme. The two schemes offer significantly more sophisticated representation of conversion from cloud water to drizzle (note that both schemes use prescribed cloud droplet concentration of 300 cm^{-3}). The two simulations resulted in some modifications of results from REF simulation, arguably because of the modified forcings from cloud-scale processes on the larger-scale flow. In particular, profiles of the horizontal flow and cloud water were significantly affected, but θ and q_v profiles were modified only in a minor way.

Increasing the horizontal resolution from 9 km (outer domain) to 3 km (inner domain) also had little impact on the solutions, with the effect on the profiles similar to that due to the vertical resolution (not shown). Note that only profiles at locations 4, 5 and 6 could be compared for the nested simulations because other locations were outside the inner domain.

**Limited-area
modelling of
stratocumulus over
South-Eastern Pacific**

M. Andrejczuk et al.

[Title Page](#)[Abstract](#)[Introduction](#)[Conclusions](#)[References](#)[Tables](#)[Figures](#)[Back](#)[Close](#)[Full Screen / Esc](#)[Printer-friendly Version](#)[Interactive Discussion](#)

The overall conclusion from the comparison between the observations and the model simulations presented above is that the WRF model was not able to simulate the observed depth of the well-mixed stratocumulus-topped subtropical boundary layer off the South American continent. We believe that there are two causes. Firstly, the input of GFS data that are used to provide the initial and lateral boundary conditions for WRF simulations already have a deficient representation of the lower tropospheric structure. This is documented in Fig. 8 which shows the comparison between aircraft observations in locations 2 and 5 (shown previously in Figs. 3 and 6, respectively) and the GFS profiles on 12 November (00:00 and 12:00 UTC) and 13 November (00:00 UTC). Clearly, the GFS profiles show a boundary layer that is about half as deep as aircraft observations suggest. It is our conjecture that lack of observations over SEP region that can be assimilated into the GFS system, in combination with deficiencies of the GFS boundary-layer scheme (perhaps similar to problems with the WRF schemes as discussed below), lead to a significantly shallower boundary layer. Arguably, the WRF model should be able to increase the depth of the boundary layer from the GFS values used as initial and lateral boundary conditions. Indeed, inspection of the inversion height predicted by the WRF model (not shown) documents that the inversion height increases from the GFS values near the south-eastern inflow boundary of the inner domain (a few hundred meters) to values larger than 1 km at the western edge of the inner domain (beyond reach of the BAe-146 aircraft). The primary reason is the increase of the SST along the south-easterly flow in the inner domain (cf. Fig 1). However, as illustrated by the comparison between model output and BAe-146 observations, a boundary layer is still too shallow in the WRF simulations. This points to deficiencies in boundary layer parametrizations available in the WRF model. A comparison between the height of the boundary-layer inversion (estimated from the vertical gradient of the lower-tropospheric potential temperature profiles) and the boundary layer depth applied in the boundary layer scheme (one of many variables in WRF output) shows that the latter is significantly smaller than the former. In fact, the boundary layer depth used in the boundary-layer scheme seems to be close to the height of the cloud base.

This suggests that the change in the potential temperature gradient at the cloud base (from zero to a small positive value, the latter corresponding to the zero gradient of either the equivalent potential temperature or the liquid water potential temperature within the cloud layer) may be the reason for confusing the cloud base with the depth of the boundary layer by the scheme. This observation suggests some possible improvements to the representation of stratocumulus-topped boundary layer in the WRF model.

4.2 Formation of mesoscale cloud-free regions

Despite simulation deficiencies discussed above, an analysis focusing on the evolution of stratocumulus clouds as simulated by the limited-area WRF model was undertaken. The model simulation with 121 levels and parameterizations as in REF was used to investigate simulated development of cloud-free mesoscale regions. We use the liquid water path (LWP), the vertical integral of the liquid water content, as a convenient measure of the total condensate in each model column. Figure 9 shows spatial distribution of the LWP at 09:45, 10:45, 11:45, and 12:45 UTC (left panels) for a part of the computational domain. Corresponding distributions derived from GOES10 satellite radiances using the method of Minnis et al. (2011) as described in Wood et al. (2011b), (and averaged from GOES10 1-km resolution to model 9-km resolution) are shown in the right-hand panels. In both model simulations and in observations, LWP increases as one moves westward away from the South American continent. However, the model tends to produce higher LWP than observed in the western half of the domain, 300 to 400 g m⁻² versus the observed 100 to 200 g m⁻². The extremely high satellite-derived values at 11:45 UTC in the westward half of the domain occur approximately at sunrise and are erroneous because of the problem with retrieval of the cloud effective radius in situations with high solar zenith angles (Allen et al., 2011). Perhaps not surprisingly, the spatial variability is different in the observations and in the model, with NW-SE “streets” apparent in the model and finer-scale structures present in the observations. The latter is even more evident in the original GOES10 data, that is, prior to the spatial averaging (not shown). Finally, satellite data seem to show a significant decrease

Limited-area modelling of stratocumulus over South-Eastern Pacific

M. Andrejczuk et al.

Title Page

Abstract

Introduction

Conclusions

References

Tables

Figures



Back

Close

Full Screen / Esc

Printer-friendly Version

Interactive Discussion



of the LWP between 09:45 and 12:45 UTC (disregarding 11:45 data), possibly due to solar heating. This effect is significantly weaker (perhaps absent) in the WRF model results.

Despite different spatial patterns, both observations and simulations show regions of reduced LWP embedded within larger-scale regions of higher LWP. In the model, unlike in the observations, a few cloud-free regions develop over time. One of these forms around 10:00 UTC near 18° S and 80° W, and grows with time reaching a size between 20 000 and 30 000 km² by 12:45 UTC. No cloud clearing as pronounced as this in the numerical model, is present in satellite LWP, but there are areas with low LWP, south-east from the model-simulated clearing (i.e. near 21° S and 78° W). Satellite derived and spatially-averaged LWP may not be a good indicator of the formation of cloud-free regions (e.g. those associated with the change from closed to open cell circulation structures). Better information is provided by the 1-km-resolution GOES10 reflectance shown in Fig. 10 for 11:45 and 12:45 UTC. The figure shows an area near 21° S and 78° W that appears to be a POC. The area expands with time and moves in the south-west direction, similar to the cloud-free regions in the model.

Limited satellite data leaves numerical model results as the main source of information about lower tropospheric processes. It is unclear, however, whether the structures produced by the model and those observed have a similar genesis. Moreover, the complexity of the interactions between the simulated processes (especially those resolved and those parameterized) makes process-level understanding of model results as a significant challenge. As illustrated by the model results shown in Fig. 10, the large-scale pattern does not move significantly in space and thus the analysis can be carried out for fixed spatial locations. Three locations were chosen from the computational domain. The first one (P1) is located at 18.62° S and 79.66° W where the cloud-free region first develops. The second location (P2) at 18.62° S and 82.32° W is to the west of P1 and here the cloud-free region develops later than for P1. The third location (P3) is to the north-west of P1, 15.82° S and 82.32° W. At P3 the cloud-free region does not develop within the analysed time period. These locations are marked in Fig. 9.

Limited-area modelling of stratocumulus over South-Eastern Pacific

M. Andrejczuk et al.

[Title Page](#)[Abstract](#)[Introduction](#)[Conclusions](#)[References](#)[Tables](#)[Figures](#)[Back](#)[Close](#)[Full Screen / Esc](#)[Printer-friendly Version](#)[Interactive Discussion](#)

**Limited-area
modelling of
stratocumulus over
South-Eastern Pacific**

M. Andrejczuk et al.

[Title Page](#)[Abstract](#)[Introduction](#)[Conclusions](#)[References](#)[Tables](#)[Figures](#)[⏪](#)[⏩](#)[◀](#)[▶](#)[Back](#)[Close](#)[Full Screen / Esc](#)[Printer-friendly Version](#)[Interactive Discussion](#)

Figure 11 shows the evolution (between 02:00 and 18:00 UTC) of parameters of interest for the cloud-free region development. This include the LWP and precipitation water path (PWP), the vertical velocity averaged between 0.5 and 1.2 km (referred to as w_{int}), the inversion height (defined as the level of the maximum of the lower-tropospheric potential temperature gradient) and the boundary layer height as predicted by the WRF model. Evolution of the latter two parameters illustrate the issues already highlighted in the previous discussion. Another pertinent observation is that periods of significant drizzle (high PWP) correspond to increased LWP independently of whether the cloud-free regions develop or not.

Figure 11a shows the evolution of the parameters for location P1. A cloud-free region POC_1 develops at this location at around 10:00 UTC and lasts only about 1.5 h. As indicated by the PWP, drizzle is present at this location up to 1.5 h before cloud disappearance, but the disappearance seems to result from a strong (up to about 4 cm s^{-1} , not shown) subsidence in the model column. One cannot rule out the possibility that subsidence was initiated by drizzle evaporation because the subsidence starts at the end of the drizzle period. However, the subsidence amplifies during the period without drizzle and only then is the LWP reduced to zero. Similar evolution is apparent for the P2 location (Fig. 11b) between 12:00 and 16:00 UTC (region POC_2), with the subsidence intensifying after a period with nonzero PWP. For the two other periods NO_POC_1 in Fig. 11b and NO_POC_2 in Fig. 11c with significant subsidence, the cloud-free regions do not develop. The subsidence, with magnitudes comparable to POC_1 and POC_2 events, only leads to the reduction of LWP (suggesting reduction of the cloud depth) and suppression of drizzle. Note that the subsidence phase associated with the NO_POC_1 is separated from the similar evolution during the POC_2 phase by a significant updraft, cloud deepening, and drizzle. In general, Fig. 11 shows a significant variability and tight coupling between lower-tropospheric vertical velocity, cloud water and drizzle. Periods of significant lower tropospheric updrafts typically lead to cloud deepening and enhanced drizzle, whereas periods of significant downdrafts occasionally lead to complete cloud evaporation and formation of cloud-free regions.

**Limited-area
modelling of
stratocumulus over
South-Eastern Pacific**

M. Andrejczuk et al.

Title Page

Abstract

Introduction

Conclusions

References

Tables

Figures



Back

Close

Full Screen / Esc

Printer-friendly Version

Interactive Discussion



Coupling illustrated in Fig. 11 may be associated with mesoscale variability, for instance, due to gravity or inertia-gravity waves, affecting processes near the boundary layer top. This is further illustrated by Fig. 12 which shows vertical and horizontal cross-sections of the simulated lower troposphere with the emphasis on the flow and cloud structures. As Fig. 11 suggest, formation of cloud-free regions in the model involves a period of significant drizzle (limiting the condensed water in the cloud) followed by a strong lower-tropospheric subsidence. To illustrate spatial variability that accompanies temporal variability illustrated in Fig. 11, we show in the left panels of Fig. 12, the evolution of the LWP contour of 1 g m^{-2} (thick black line) and the vertical velocity at about 1 km height (model level 14; colors). Additionally, the direction of the horizontal wind for model levels below and above the boundary layer inversion (model levels 12 and 19; about 0.8 and 1.3 km height) are shown using gray and magenta arrows, respectively. The figure shows that the model simulates an organized mesoscale pattern of lower-tropospheric vertical velocity (updrafts and downdrafts), approximately along the SE-NW direction. Cloud-free regions form in subsidence areas and the cloud-free region in the center of the domain expands as the subsidence in this area expands. There is also a significant change of the horizontal velocity direction between the boundary layer and the free troposphere, covering most of the domain shown, with the wind changing direction from S-E (within the boundary layer) to E above. A strong subsidence (up to 8 cm s^{-1}) seems to be associated with the wind convergence above the boundary layer. A large organized updraft region forms later (panel d) along the northern edge of the cloud-free region.

The right panels of Fig. 12 show vertical cross sections along the latitude of 18.62° S . The vertical velocity responsible for the cloud clearing is mostly limited to the lowest 2 km of the atmosphere. The pattern of the vertical velocity seems to be directly associated with the cloud depth pattern, with regions of updraft/downdraft coinciding with deeper/shallower clouds. As already illustrated by horizontal cross-sections in the left hand panels, the vertical velocity pattern does not seem to be associated with any coherent structures, such as gravity or inertia-gravity waves.

**Limited-area
modelling of
stratocumulus over
South-Eastern Pacific**

M. Andrejczuk et al.

[Title Page](#)[Abstract](#)[Introduction](#)[Conclusions](#)[References](#)[Tables](#)[Figures](#)[Back](#)[Close](#)[Full Screen / Esc](#)[Printer-friendly Version](#)[Interactive Discussion](#)

Entrainment of the free-tropospheric air into the cloud-topped boundary layer may also play some role in the formation of cloud-free regions. Figure 13 shows vertical cross-sections of the potential temperature and q_v fields in the vicinity of the boundary layer inversion for the same times and locations as in Fig. 12. As the figure shows, the temperature and moisture fields show a significant horizontal variability in the vicinity of the inversion, with strong horizontal jumps of the temperature contours and associated variability of the vertical temperature and moisture gradients. Arguably, such variability may be related to entrainment events, although relatively low vertical resolution may play some role as well. The black rectangles in Fig. 13 indicates a zone of enhanced horizontal and vertical gradients as it passes the location P1 at the time when the cloud-free region develops. At approximately the same time, subsidence at the location P2 is observed, but a cloud-free region does not develop. It is perhaps relevant that in the vicinity of P2 the horizontal and vertical gradients near the boundary layer inversion are not as strong as near P1. But when warmer and drier air passes over location P2 later (i.e. POC_2 time in Fig. 11), the cloud-free region does form. This specific example suggests that entrainment and mixing, in addition to subsidence alone, may be required to completely evaporate the cloud.

The evolution of lower-tropospheric profiles within the four regions (POC_1, POC_2, NO_POC_1, and NO_POC_2) are presented in Figs. 14 to 17, respectively. The profiles are shown in 30-min intervals starting at 08:30/13:15/08:15/04:00 UTC for POC_1/POC_2/NO_POC_1/NO_POC_2. There are a few common features for all the profiles. Firstly, as already illustrated, there is an inversion separating the boundary layer from the free troposphere evident in the temperature, moisture and horizontal velocity profiles. The boundary layer is approximately well-mixed for total water and liquid water potential temperature and for the horizontal wind components. Secondly, the extrema of the lower-tropospheric vertical velocity are typically located near the cloud top. The maxima seem similar for the POC and NO_POC profiles. Perhaps the most significant differences are in the depth of the cloud layer, shallower in the POC case (Figs. 13 and 14) and deeper in the NO_POC case (Figs. 15 and 16). Presence/absence of

**Limited-area
modelling of
stratocumulus over
South-Eastern Pacific**

M. Andrejczuk et al.

[Title Page](#)[Abstract](#)[Introduction](#)[Conclusions](#)[References](#)[Tables](#)[Figures](#)[Back](#)[Close](#)[Full Screen / Esc](#)[Printer-friendly Version](#)[Interactive Discussion](#)

boundary layer scheme confused the cloud base (where the temperature and moisture profiles change from no-gradient below to a weak gradient above) with the boundary-layer inversion near the cloud top, where large gradients of temperature and moisture are typically present. This implies that the surface heat, moisture, and momentum fluxes in the model are likely to be distributed over a significantly thinner layer compared to observations. This in turn leads to a shallow boundary layer with low cloud base and cloud top height. Model solutions changed little when the number of model levels was increased from 36 to 81 and when the horizontal gridlength was reduced from 9 km to 3 km for the 36-level simulation. Moreover, they also changed little when different boundary-layer and cloud microphysics parametrizations were used.

An analysis was carried out for three different locations and it was shown that the cloud-free regions were created as a result of the interaction between regions of lower-tropospheric mesoscale subsidence (a maximum downdraft velocity of a few cm s^{-1}) possibly accompanied by entrainment (of dry and warm free-tropospheric air into boundary layer) with parameterized cloud-topped boundary layer processes (such as boundary-layer transports and condensation/evaporation). Drizzle, limiting the cloud liquid water content and the cloud water path, might play some role, but it typically ceased one to two hours before the cloud-free region had been formed. Note that this is generally consistent with observational study of Allen et al. (2011) where the passage of a mesoscale inertia-gravity wave was argued to be responsible for the transition from fully-cloudy closed-cell circulation patterns to the partially-cloudy open-cell structures. However, Allen et al. (2011) hypothesized quite a different chain of events leading to the transition. They argued that the deepening of the cloud field leads to more drizzle, and the enhanced drizzle results in the transition. Such a picture is consistent with previous LES studies (e.g. Savic-Jovicic and Stevens, 2008) suggesting that strongly-drizzling stratocumulus with closed-cell circulations gradually transitions into open cells. Small-scale dynamical processes associated with the drizzle fallout and evaporation, unresolved in the limited area model, are likely to be key in the transition. The WRF simulations discussed here show direct evaporation of the cloud due to

lower-tropospheric mesoscale subsidence and possibly entrainment/mixing with little, if any, role of drizzle. It is thus not surprising that the formation of cloud-free regions was relatively insensitive to the parameterization of cloud microphysics.

Model results reported here call for further studies using LES models applying time-evolving vertical velocity due to lower-tropospheric waves as in Allen et al. (2011) or mesoscale features simulated in the current study. Such simulations should document if the evolution hypothesized in Allen et al. (2011) and simulated by limited-area model reported here are indeed reproduced by a model that resolves boundary-layer dynamics as well as cloud and drizzle processes. We hope to report on such simulations in the near future.

Acknowledgements. This work was supported by NERC funding for the VOCALS-REx project, NCAS computer time on HECToR, and BADC data centre. WWG was partially supported by the NOAA grant NA08OAR4310543 and DOE ARM grant DE-FG02-08ER64574. LWP data derived from GOES10 was provided by P. Minnis.

References

- Abel, S. J., Walters, D. N., and Allen, G.: Evaluation of stratocumulus cloud prediction in the Met Office forecast model during VOCALS-REx, *Atmos. Chem. Phys.*, 10, 10541–10559, doi:10.5194/acp-10-10541-2010, 2010. 25520
- Allen, G., Vaughan, G., Coe, H., and Minnis, P.: Gravity waves observed as a causal mechanism for transition from closed to open cellular convection in the remote South East Pacific, to be submitted, 2011. 25529, 25535, 25536
- Minnis, P., Sun-Mack, S., Young, D. F., Heck, P. W., Garber, D. P., Chen, Y., Spangenberg, D. A., Arduini, R. F., Trepte, Q. Z., Jr., W. L. S., Ayers, J. K., Gibson, S. C., Miller, W. F., Chakrapani, V., Takano, Y., Liou, K.-N., Xie, Y., and Yang, P.: CERES Edition-2 cloud property retrievals using TRMM VIRS and Terra and Aqua MODIS data, Part I: Algorithms, *IEEE T. Geosci. Remote Sens.*, in press, 2011. 25529
- Morrison, H., Thompson, G., and Tatarskii, V.: Impact of cloud microphysics on the development of trailing stratiform precipitation in a simulated squall line: Comparison of one- and two-moment schemes, *Mon. Weather Rev.*, 137, 991–1007, 2009. 25527

25536

ACPD

11, 25517–25556, 2011

Limited-area modelling of stratocumulus over South-Eastern Pacific

M. Andrejczuk et al.

Title Page

Abstract

Introduction

Conclusions

References

Tables

Figures



Back

Close

Full Screen / Esc

Printer-friendly Version

Interactive Discussion



Limited-area modelling of stratocumulus over South-Eastern Pacific

M. Andrejczuk et al.

[Title Page](#)[Abstract](#)[Introduction](#)[Conclusions](#)[References](#)[Tables](#)[Figures](#)[⏪](#)[⏩](#)[◀](#)[▶](#)[Back](#)[Close](#)[Full Screen / Esc](#)[Printer-friendly Version](#)[Interactive Discussion](#)

- Petters, M. D., Snider, J. R., Stevens, B., Vali, G., Faloon, I., and Russell, L. M.: Accumulation mode aerosol, pockets of open cells, and particle nucleation in the remote subtropical Pacific marine boundary layer, *J. Geophys. Res.*, 111, D02206, doi:10.1029/2004JD005694, 2006. 25520
- 5 Rahn, D. A. and Garreaud, R.: Marine boundary layer over the subtropical southeast Pacific during VOCALS-REx – Part 1: Mean structure and diurnal cycle, *Atmos. Chem. Phys.*, 10, 4491–4506, doi:10.5194/acp-10-4491-2010, 2010. 25519
- Savic-Jovicic, V. and Stevens, B.: The structure and mesoscale organization of precipitating stratocumulus, *J. Atmos. Sci.*, 65, 1587–1605, 2008. 25520, 25535
- 10 Sharon, T. M., Albrecht, B. A., Jonsson, H. H., Minnis, P., Khaiyer, M. M., van Reken, T. M., Seinfeld, J., and Flagan, R.: Aerosol and Cloud Microphysical Characteristics of Rifts and Gradients in Maritime Stratocumulus Clouds, *J. Atmos. Sci.*, 63, 983–997, 2006. 25519, 25520
- Skamarock, W. C., Klemp, J. B., Dudhia, J., Gill, D. O., Barker, D. M., Duda, M. G., Huang, X.-Y., Wang, W., and Powers, J. G.: A Description of the Advanced Research WRF Version 3, National Center for Atmospheric Research, 2008. 25521, 25524, 25539
- Stevens, B., Vali, G., Comstock, K., Wood, R., VanZanten, M. C., Austin, P. H., Bretherton, C. S., and Lenschow, D. H.: Pockets of open cells and drizzle in marine stratocumulus, *B. Am. Meteor. Soc.*, 86, 51–57, 2005. 25519
- 20 Thompson, G., Rasmussen, R. M., and Manning, K.: Explicit forecasts of winter precipitation using an improved bulk microphysics scheme. Part I: Description and sensitivity analysis, *Mon. Weather Rev.*, 132, 519–542, 2004. 25527
- Toniazzo, T., Abel, S. J., Wood, R., Mechoso, C. R., Allen, G., and Shaffrey, L. C.: Large-scale and synoptic meteorology in the South-East Pacific during the observations campaign VOCALS-REx in Spring 2008, *Atmos. Chem. Phys. Discuss.*, 11, 225–288, doi:10.5194/acpd-11-225-2011, 2011. 25519
- 25 VanZanten, M. C. and Stevens, B.: Observations of the Structure of Heavily Precipitating Marine Stratocumulus, *J. Atmos. Sci.*, 62, 4327–4342, 2005. 25520
- Wang, H. and Feingold, G.: Modeling Mesoscale Cellular Structures and Drizzle in Marine Stratocumulus. Part I: Impact of Drizzle on the Formation and Evolution of Open Cells, *J. Atmos. Sci.*, 66, 3237–3256, 2009a. 25520
- 30 Wang, H. and Feingold, G.: Modeling Mesoscale Cellular Structures and Drizzle in Marine Stratocumulus. Part I: Impact of Drizzle on the Formation and Evolution of Open Cells, *J.*

Limited-area modelling of stratocumulus over South-Eastern Pacific

M. Andrejczuk et al.

Title Page

Abstract

Introduction

Conclusions

References

Tables

Figures

⏪

⏩

◀

▶

Back

Close

Full Screen / Esc

Printer-friendly Version

Interactive Discussion



Atmos. Sci., 66, 3237–3256, 2009b. 25520

Wang, H., Feingold, G., Wood, R., and Kazil, J.: Modelling microphysical and meteorological controls on precipitation and cloud cellular structures in Southeast Pacific stratocumulus, Atmos. Chem. Phys., 10, 6347–6362, doi:10.5194/acp-10-6347-2010, 2010. 25520

5 Wood, R., Comstock, K. K., Bretherton, C. S., Cornish, C., Tomlinson, J., Collins, D. R., and Fairall, C.: Open cellular structure in marine stratocumulus sheets, J. Geophys. Res., 113, D12207, doi:10.1029/2007JD009371, 2008. 25520

10 Wood, R., Bretherton, C. S., Leon, D., Clarke, A. D., Zuidema, P., Allen, G., and Coe, H.: An aircraft case study of the spatial transition from closed to open mesoscale cellular convection over the Southeast Pacific, Atmos. Chem. Phys., 11, 2341–2370, doi:10.5194/acp-11-2341-2011, 2011a. 25520

15 Wood, R., Mechoso, C. R., Bretherton, C. S., Weller, R. A., Huebert, B., Straneo, F., Albrecht, B. A., Coe, H., Allen, G., Vaughan, G., Daum, P., Fairall, C., Chand, D., Gallardo Klenner, L., Garreaud, R., Grados, C., Covert, D. S., Bates, T. S., Krejci, R., Russell, L. M., de Szoeke, S., Brewer, A., Yuter, S. E., Springston, S. R., Chaigneau, A., Toniazzo, T., Minnis, P., Palikonda, R., Abel, S. J., Brown, W. O. J., Williams, S., Fochesatto, J., Brioude, J., and Bower, K. N.: The VAMOS Ocean-Cloud-Atmosphere-Land Study Regional Experiment (VOCALS-REx): goals, platforms, and field operations, Atmos. Chem. Phys., 11, 627–654, doi:10.5194/acp-11-627-2011, 2011b. 25519, 25529

Limited-area modelling of stratocumulus over South-Eastern Pacific

M. Andrejczuk et al.

Table 1. Physical parametrizations used in the simulations with WRF model version 3 (Skamarock et al., 2008). Exactly the same parametrizations were used for outer and inner domain.

Run	REF	SM1	SM2	SF1	SF2
Physics	Option (name)	Option (name)	Option (name)	Option (name)	Option (name)
mp_physics	1 (Kessler)	8 (Thompson)	10 (Morrison)		
ra_lw_physics	1 (RRTM)				
ra_sw_physics	2 (Goddard)				
sf_sfclay_physics	7 (Pleim-Xiu)			1 (Monin-Obukhov)	2 (Monin-Obukhov (ETA))
sf_surface_physics	2 (Noah)			1 (thermal diffusion)	1 (thermal diffusion)
bl_pbl_physics	7 (ACM2)			1 (YSU)	2 (MYJ TKE)
cu_physics	0 (cumulus option)				
sst_update	1 (SST)				

Title Page

Abstract

Introduction

Conclusions

References

Tables

Figures

⏪

⏩

◀

▶

Back

Close

Full Screen / Esc

Printer-friendly Version

Interactive Discussion

**Limited-area
modelling of
stratocumulus over
South-Eastern Pacific**

M. Andrejczuk et al.

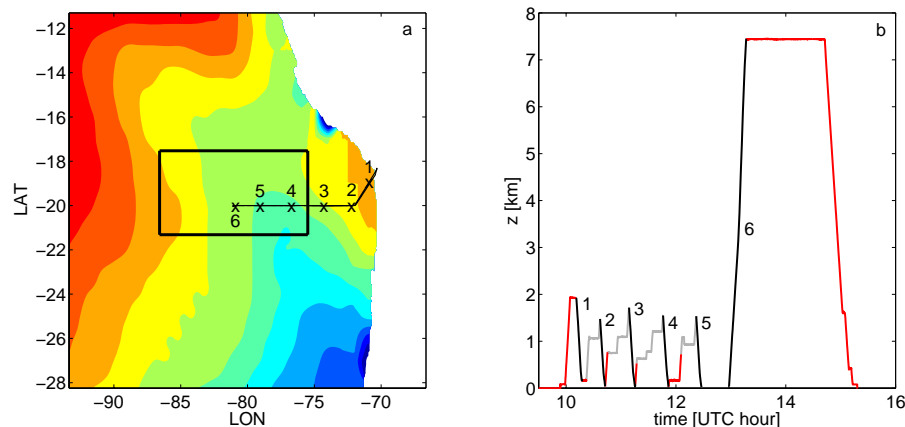


Fig. 1. Aircraft track for the flight B420. Left panel: WRF domain and geographical position of the aircraft together with the SST (colors) and WRF inner domain (black rectangle). Right panel: aircraft altitude versus time for the track shown in the left panel; black lines – profiles used for model evaluation, gray lines – additional segments used to document the lower-tropospheric variability within the observed system.

[Title Page](#)[Abstract](#)[Introduction](#)[Conclusions](#)[References](#)[Tables](#)[Figures](#)[◀](#)[▶](#)[◀](#)[▶](#)[Back](#)[Close](#)[Full Screen / Esc](#)[Printer-friendly Version](#)[Interactive Discussion](#)

**Limited-area
modelling of
stratocumulus over
South-Eastern Pacific**

M. Andrejczuk et al.

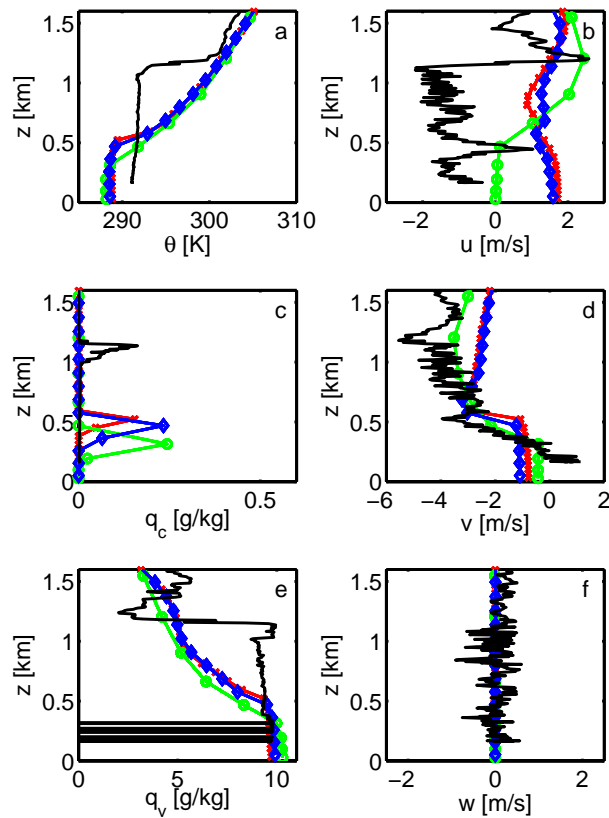


Fig. 2. Model sensitivity to the number of vertical levels for the profile 1, black line – observations, green – model run with 36 vertical levels, blue – model run with 81 vertical levels, red – model run with 121 vertical levels.

[Title Page](#)[Abstract](#)[Introduction](#)[Conclusions](#)[References](#)[Tables](#)[Figures](#)[◀](#)[▶](#)[◀](#)[▶](#)[Back](#)[Close](#)[Full Screen / Esc](#)[Printer-friendly Version](#)[Interactive Discussion](#)

Limited-area modelling of stratocumulus over South-Eastern Pacific

M. Andrejczuk et al.

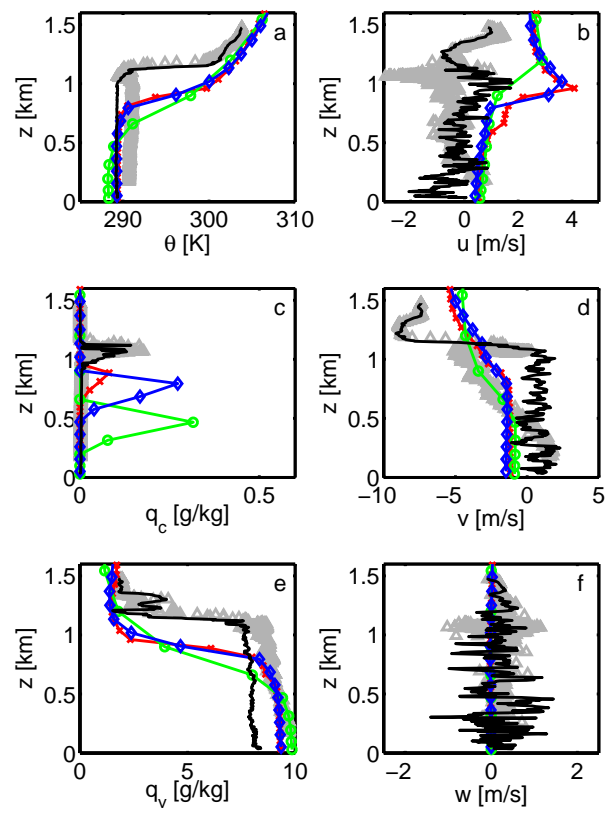


Fig. 3. As Fig. 2 but for profile 2; gray points – variability of measurements.

Title Page

Abstract

Introduction

Conclusions

References

Tables

Figures

◀

▶

◀

▶

Back

Close

Full Screen / Esc

Printer-friendly Version

Interactive Discussion



**Limited-area
modelling of
stratocumulus over
South-Eastern Pacific**

M. Andrejczuk et al.

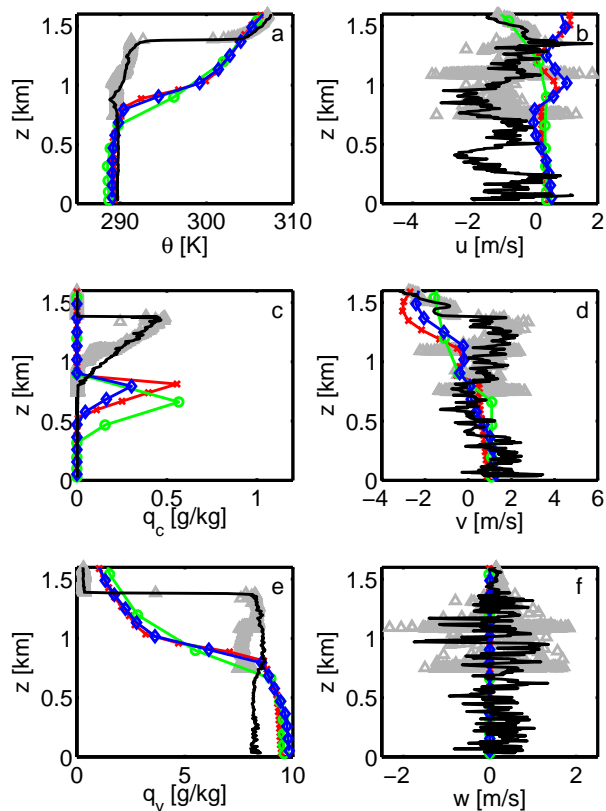


Fig. 4. As Fig. 2 but for profile 3; gray points – variability of measurements.

Title Page

Abstract

Introduction

Conclusions

References

Tables

Figures

◀

▶

◀

▶

Back

Close

Full Screen / Esc

Printer-friendly Version

Interactive Discussion



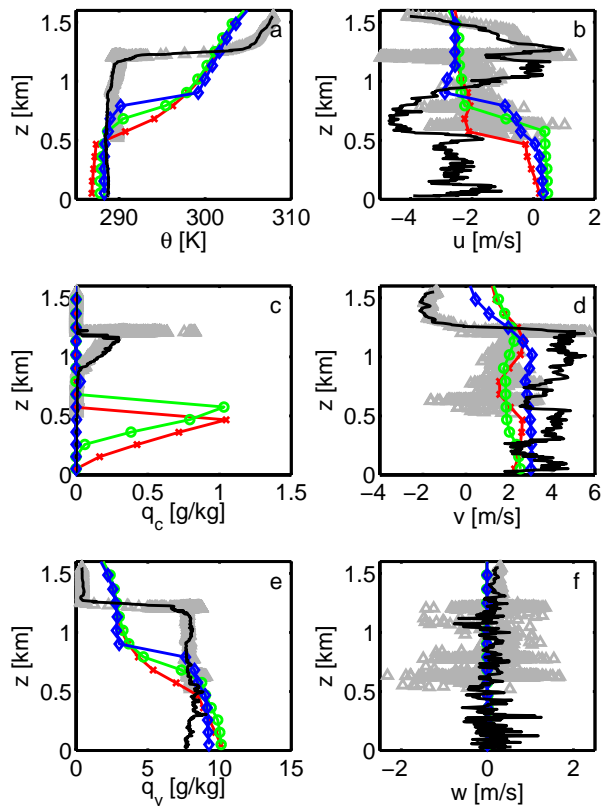


Fig. 5. Model sensitivity to the boundary layer parametrizations for the run with 81 vertical levels, for profile 4; black line – observations, blue – run REF, green – run SF1, red – run SF2; gray points – variability of measurements.

**Limited-area
modelling of
stratocumulus over
South-Eastern Pacific**

M. Andrejczuk et al.

Title Page

Abstract

Introduction

Conclusions

References

Tables

Figures

◀

▶

◀

▶

Back

Close

Full Screen / Esc

Printer-friendly Version

Interactive Discussion



Limited-area modelling of stratocumulus over South-Eastern Pacific

M. Andrejczuk et al.

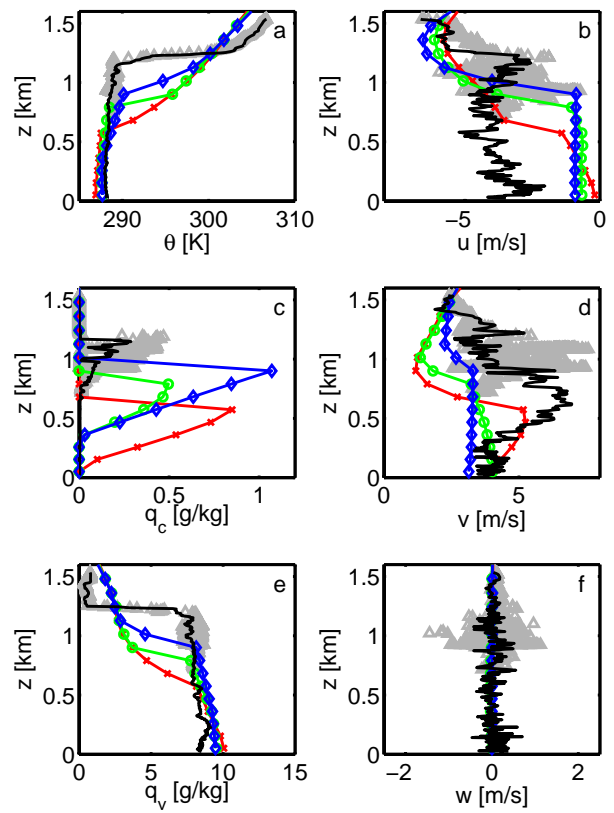


Fig. 6. As Fig. 5 but for profile 5; gray points – variability of measurements.

Title Page

Abstract

Introduction

Conclusions

References

Tables

Figures

◀

▶

◀

▶

Back

Close

Full Screen / Esc

Printer-friendly Version

Interactive Discussion



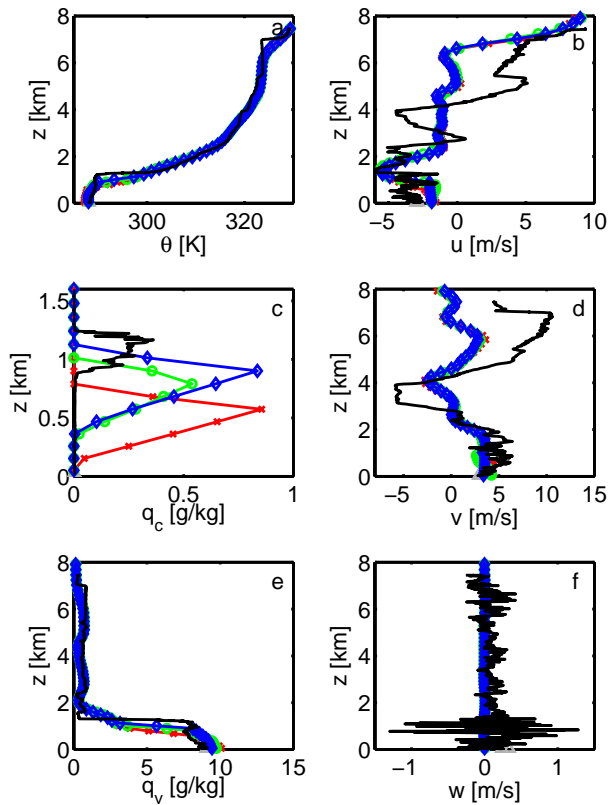


Fig. 7. As Fig. 5 but for profile 6.

Limited-area modelling of stratocumulus over South-Eastern Pacific

M. Andrejczuk et al.

Title Page

Abstract Introduction

Conclusions References

Tables Figures

◀ ▶

◀ ▶

Back Close

Full Screen / Esc

Printer-friendly Version

Interactive Discussion



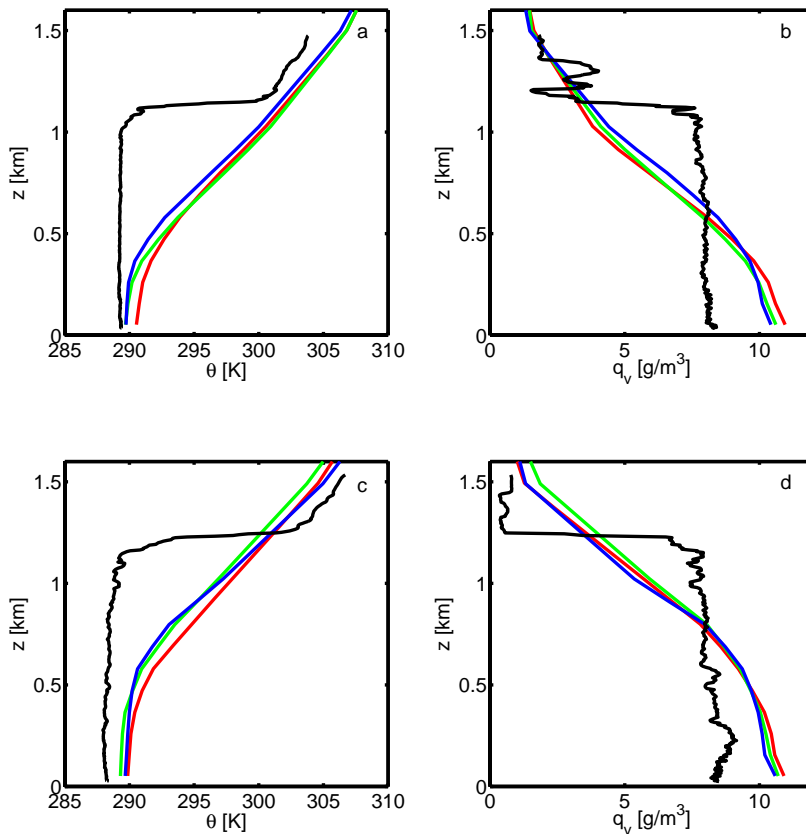


Fig. 8. GFS profiles of the θ and q_v for location 2 (upper panels) and location 5 (lower panels) for 12 November for 00:00 h – blue, 12 November for 12:00 h – green, and 13 November for 00:00 hh – red. Black lines show profiles measured by the BAE-146.

Limited-area modelling of stratocumulus over South-Eastern Pacific

M. Andrejczuk et al.

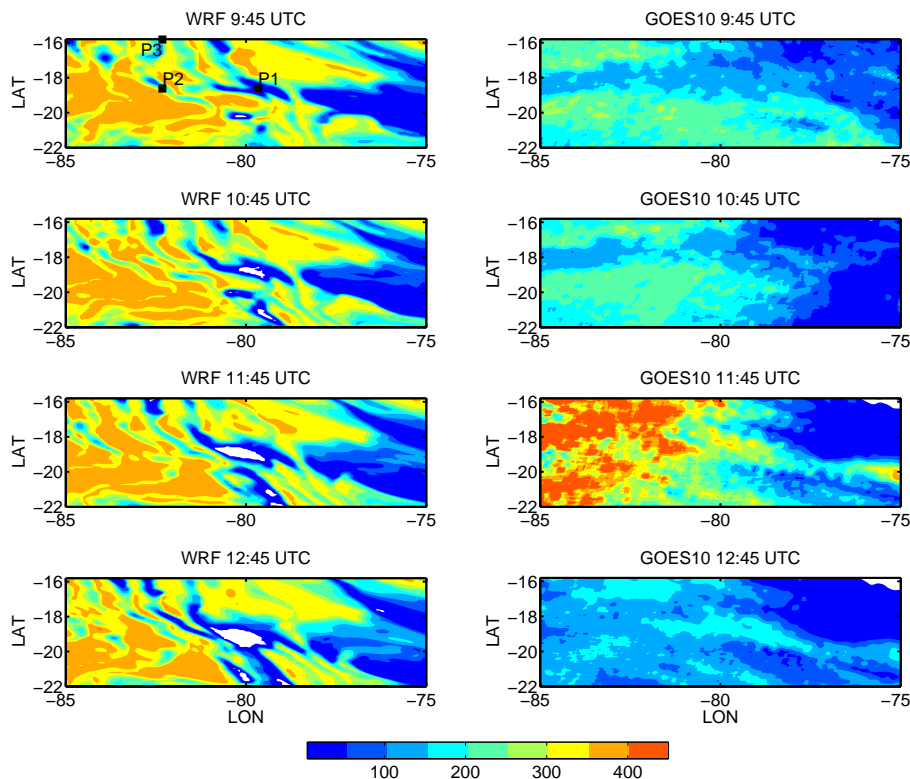


Fig. 9. Left column – LWP for the model solution with 121 vertical levels for times 09:45, 10:45, 11:45, 12:45 UTC, right column – GOES10 LWP for the same times.

Title Page

Abstract

Introduction

Conclusions

References

Tables

Figures

◀

▶

◀

▶

Back

Close

Full Screen / Esc

Printer-friendly Version

Interactive Discussion

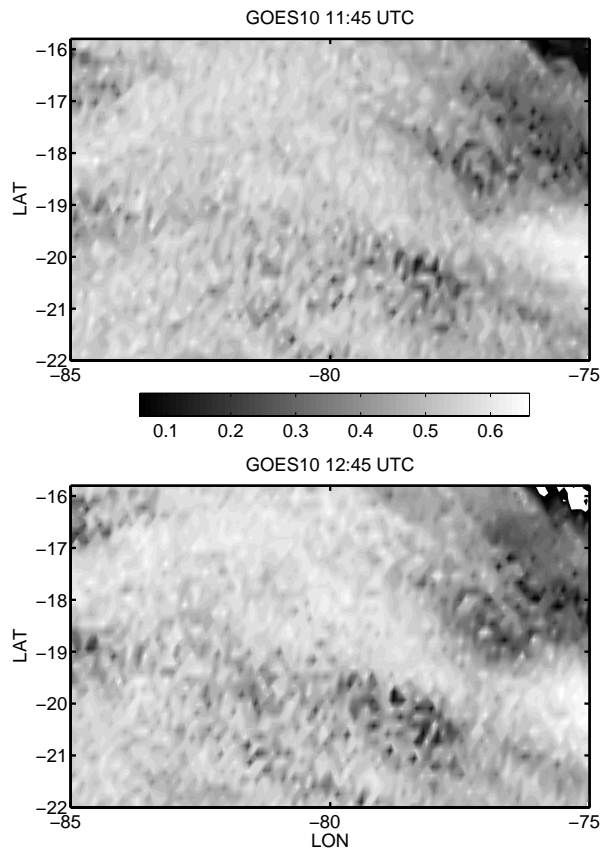


Fig. 10. GOES10 Visible reflectance for 11:45, 12:45 UTC.

**Limited-area
modelling of
stratocumulus over
South-Eastern Pacific**

M. Andrejczuk et al.

Title Page

Abstract Introduction

Conclusions References

Tables Figures

◀ ▶

◀ ▶

Back Close

Full Screen / Esc

Printer-friendly Version

Interactive Discussion



Limited-area modelling of stratocumulus over South-Eastern Pacific

M. Andrejczuk et al.

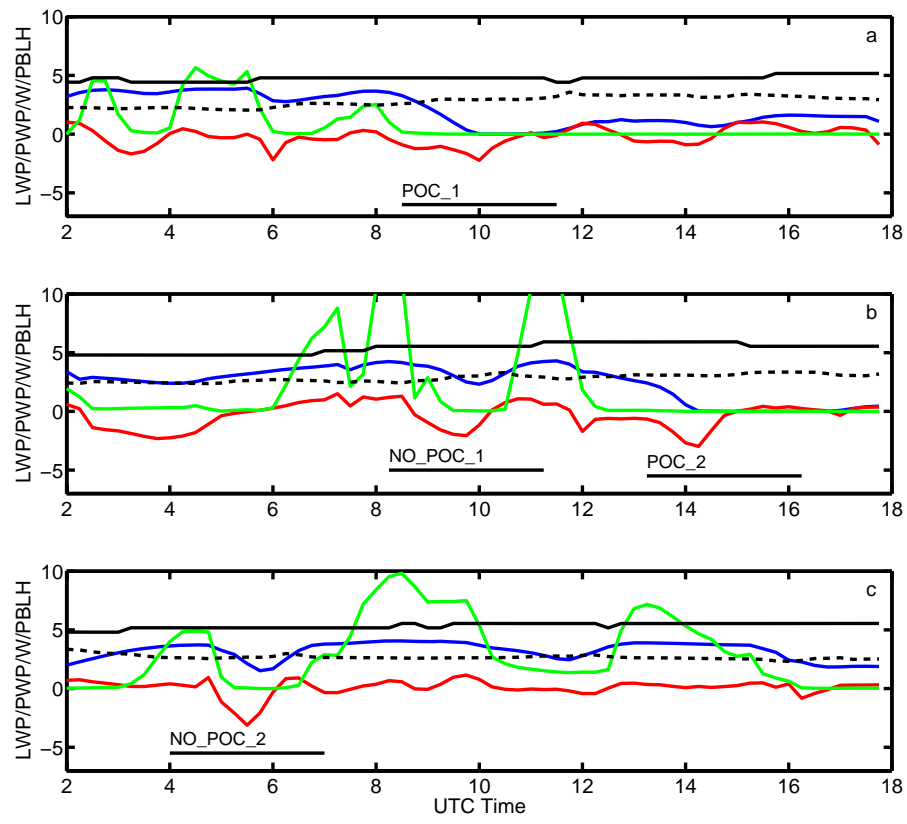


Fig. 11. Evolution in time of the LWP \times 0.01 (blue), PWP q_r (green), w_{int} (red), inversion height \times 0.005 (black solid), and boundary layer height \times 0.005 (black dashed) for location 1 ($-79.66, 18.62$) – (a), for location 2 ($-82.32, -18.62$) – (b), and for location 3 ($-82.32, -15.82$) – (c).

Title Page

Abstract Introduction

Conclusions References

Tables Figures

⏪ ⏩

◀ ▶

Back Close

Full Screen / Esc

Printer-friendly Version

Interactive Discussion



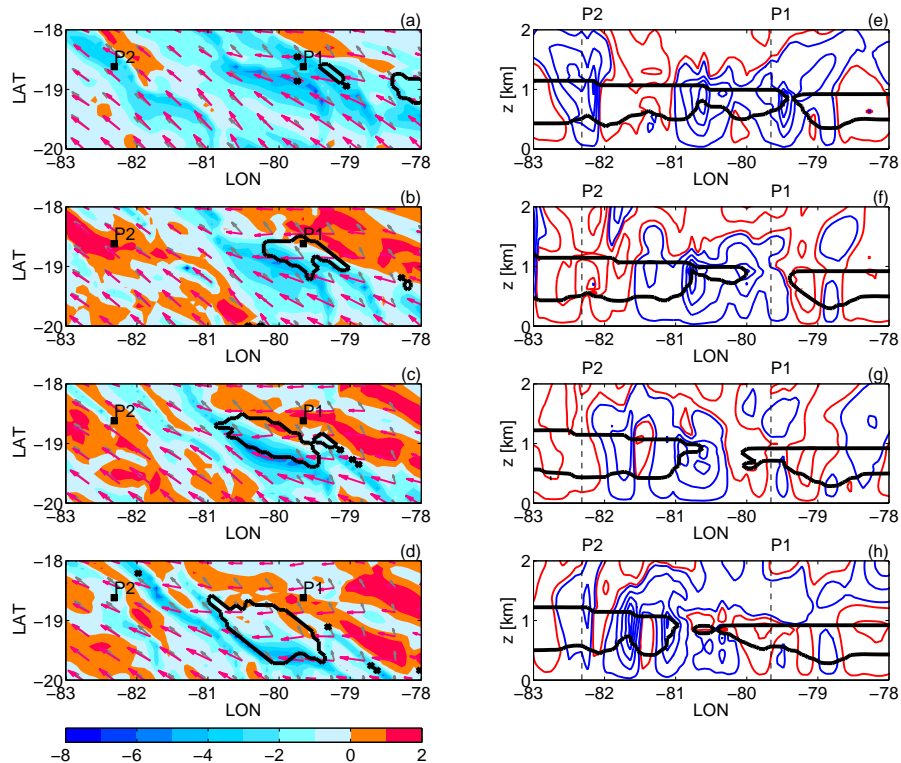


Fig. 12. Vertical velocity (in color) on level 14 ($z = 1000$ m) and 1 $[\text{g m}^{-2}]$ LWP contour (black line) for times 09:15, 10:15, 11:15, 12:15 UTC **(a–d)**; gray arrows – horizontal velocity on level 12 ($z = 780$ m), magenta arrows – horizontal velocity above the boundary layer on level 19 ($z = 1300$ m). Right column – vertical cross section through the computational domain for the latitude 18.62S. Red/blue – contours of the positive/negative vertical velocity starting from 0.2/–0.2 cm s^{-1} , every 1 cm s^{-1} . Black line – contour of the $q_c = 0.1$ g kg^{-1} , purple line – contour of $\theta = 299.5$ K.

Limited-area modelling of stratocumulus over South-Eastern Pacific

M. Andrejczuk et al.

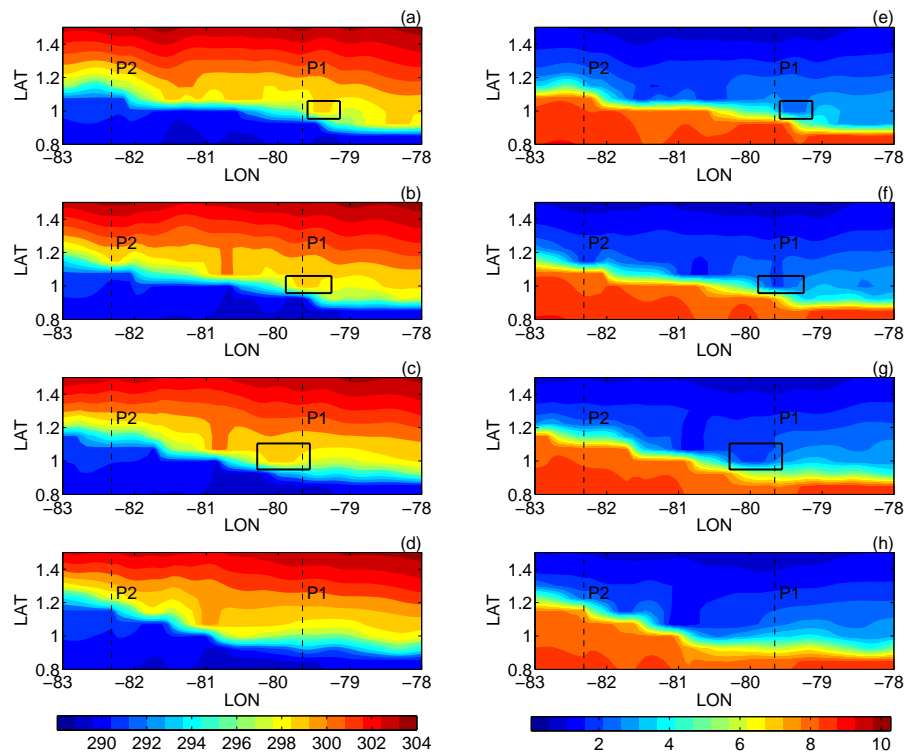


Fig. 13. Vertical cross section through the computational domain for the latitude 18.62° S, left panels – θ , right panels q_v .

Title Page

Abstract

Introduction

Conclusions

References

Tables

Figures

◀

▶

◀

▶

Back

Close

Full Screen / Esc

Printer-friendly Version

Interactive Discussion

Limited-area modelling of stratocumulus over South-Eastern Pacific

M. Andrejczuk et al.

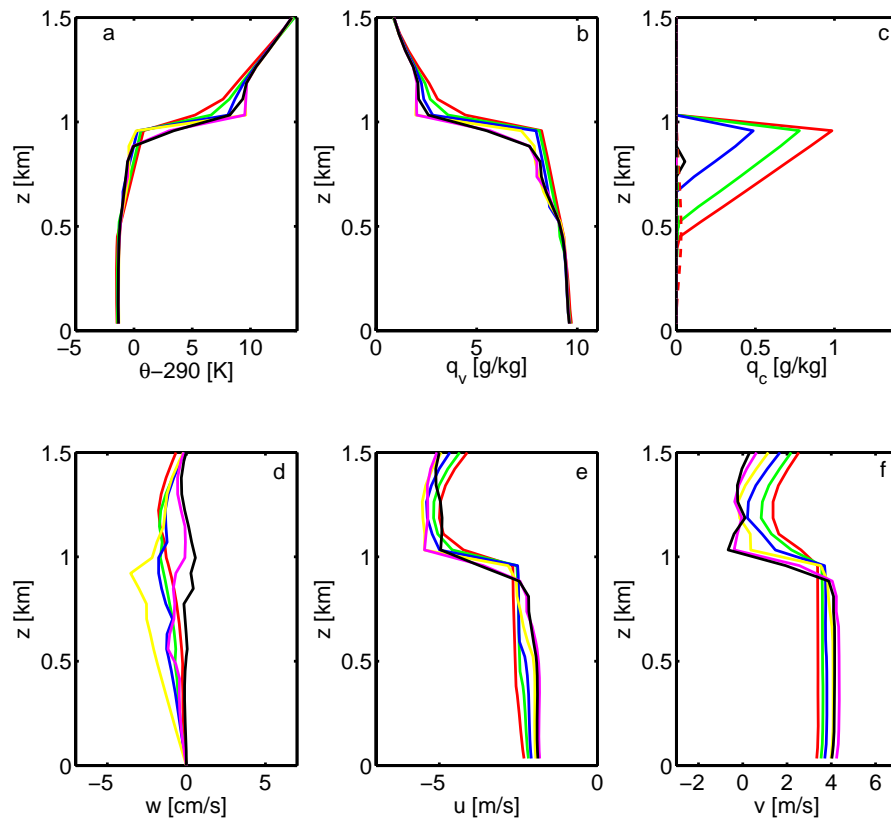


Fig. 14. Vertical profiles of θ (a), q_v (b), q_c (c), w (d), u (e), v (f) for location 1 (POC_1) for times 08:30 (red), 09:00 (green), 09:30 (blue), 10:00 (yellow), 10:30 (magenta), 11:00 (black) UTC.

[Title Page](#)
[Abstract](#)
[Introduction](#)
[Conclusions](#)
[References](#)
[Tables](#)
[Figures](#)
[◀](#)
[▶](#)
[◀](#)
[▶](#)
[Back](#)
[Close](#)
[Full Screen / Esc](#)
[Printer-friendly Version](#)
[Interactive Discussion](#)

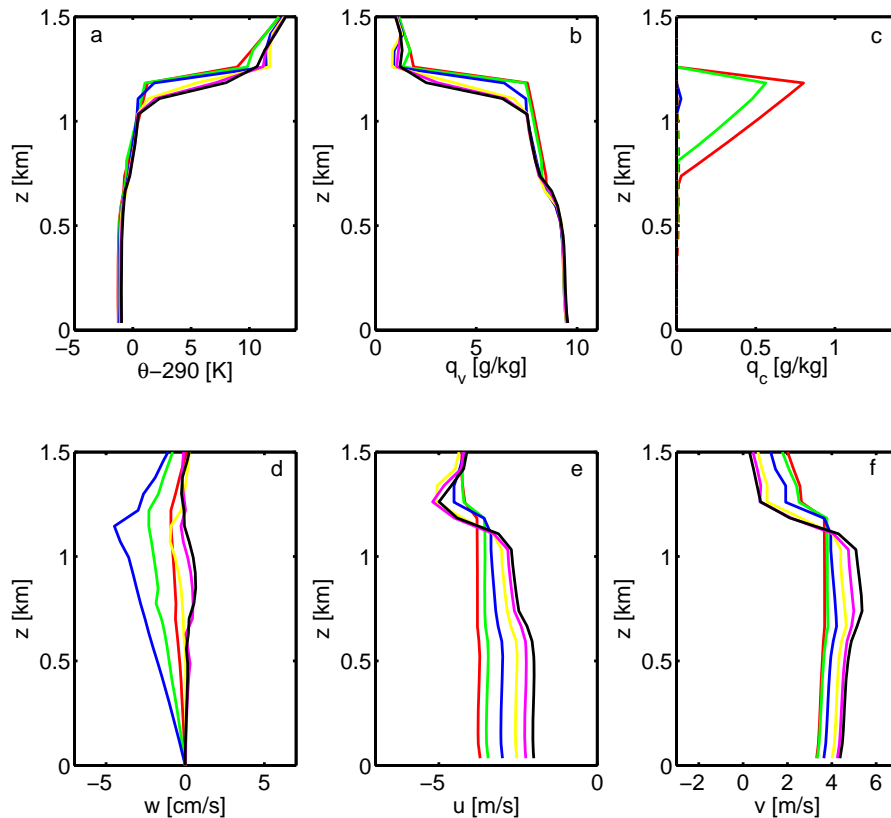


Fig. 15. Vertical profiles of θ (a), q_v (b), q_c (c), w (d), u (e), v (f) for location 2 (POC_2) for times 13:15 (red), 13:45 (green), 14:15 (blue), 14:45 (yellow), 15:15 (magenta), 15:45 (black) UTC.

**Limited-area
modelling of
stratocumulus over
South-Eastern Pacific**

M. Andrejczuk et al.

Title Page

Abstract Introduction

Conclusions References

Tables Figures

◀ ▶

◀ ▶

Back Close

Full Screen / Esc

Printer-friendly Version

Interactive Discussion



Limited-area modelling of stratocumulus over South-Eastern Pacific

M. Andrejczuk et al.

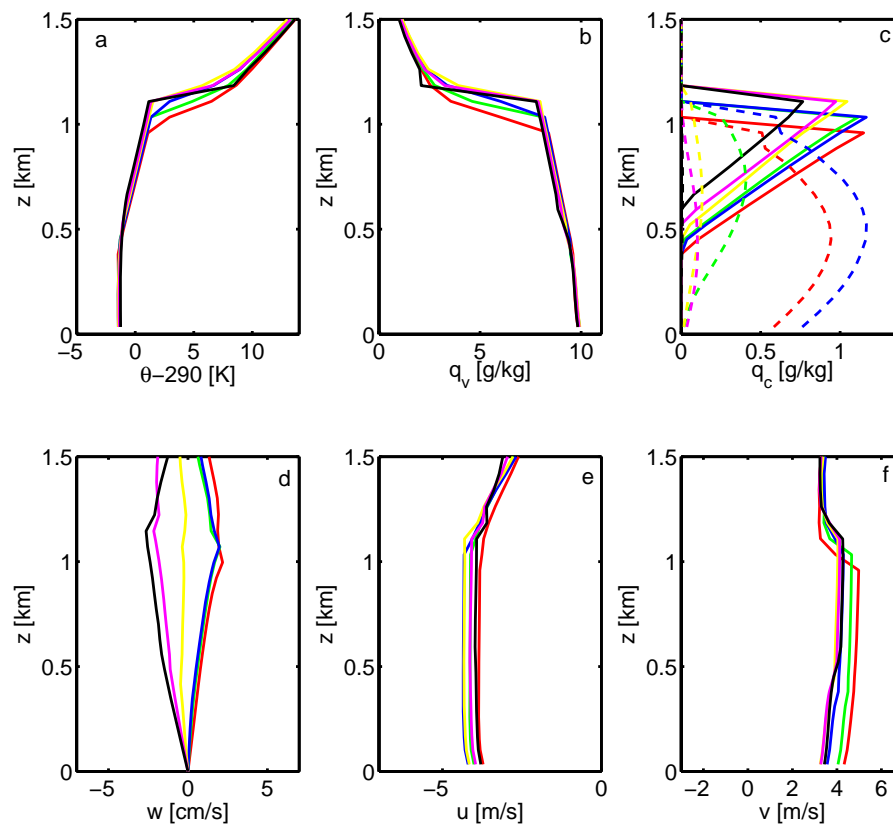


Fig. 16. Vertical profiles of θ (a), q_v (b), q_c (c), w (d), u (e), v (f) for location 2 (NO_POC_1) for times 08:15 (red), 08:45 (green), 09:15 (blue), 09:45 (yellow), 10:15 (magenta), 10:45 (black) UTC.

[Title Page](#)
[Abstract](#)
[Introduction](#)
[Conclusions](#)
[References](#)
[Tables](#)
[Figures](#)
[◀](#)
[▶](#)
[◀](#)
[▶](#)
[Back](#)
[Close](#)
[Full Screen / Esc](#)
[Printer-friendly Version](#)
[Interactive Discussion](#)

Limited-area modelling of stratocumulus over South-Eastern Pacific

M. Andrejczuk et al.

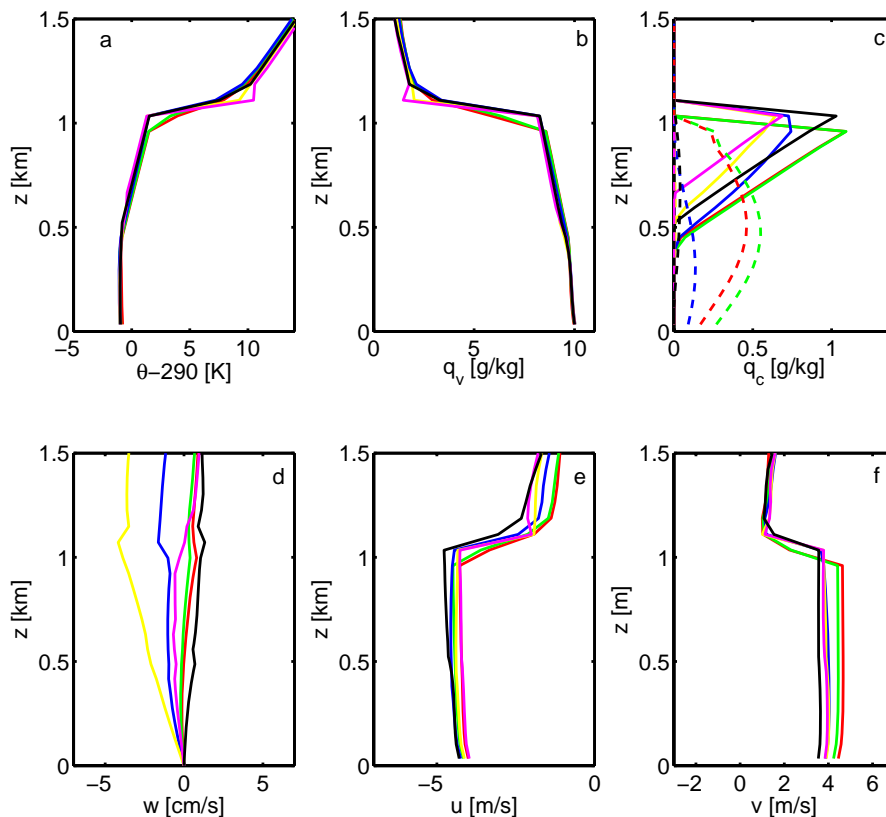


Fig. 17. Vertical profiles of θ (a), q_v (b), q_c (c), w (d), u (e), v (f) for location 3 (NO_POC_2) for times 04:00 (red), 04:30 (green), 05:00 (blue), 05:30 (yellow), 06:00 (magenta), 06:30 (black) UTC.

[Title Page](#)
[Abstract](#)
[Introduction](#)
[Conclusions](#)
[References](#)
[Tables](#)
[Figures](#)
[◀](#)
[▶](#)
[◀](#)
[▶](#)
[Back](#)
[Close](#)
[Full Screen / Esc](#)
[Printer-friendly Version](#)
[Interactive Discussion](#)